Automated Separation of Basalt Fiber and Other Earth Resources by the Means of Acoustic Vibrations

Anri Elbakian[1], *Boris Sentyakov*[1], *Pavol Božek*[2], *Ivan Kuric*[3] and *Kirill Sentyakov*[1]

The production of a composite nanostructured polymer reinforced with basalt fiber requires precise and fine separation of non-fibrous inclusions. The unique properties of such material predetermine it for use in various sectors, but especially in mining (safer for mining purposes, for example, drilling without sparkle occurrence, lower production price than metal mining tools, etc.) (Kemal Ozfirat, 2015). Basalt fiber is a material from which products with excellent thermal conductivity, hygroscopicity, and chemical resistance are obtained, in addition, they do not burn. Used in many industries, including mechanical engineering, as well as heat insulation material in the construction and other human activities. However, in the production of basalt fiber cloths, non-fibrous inclusions are formed. These inclusions reduce the quality of the products and, due to their barbs, can lead to injuries, especially of the mucous membrane. It was found in research (Timoshenko et al., 1985) that when affecting basalt fiber canvases by sound waves of the acoustic field, non-fibrous inclusions are falls from them. The task of modeling this phenomenon and process is worthwhile.

Keywords: basalt fiber, non-fiber inclusion, frequency, vibrations, sound, precise separation, mining

Introduction

Recently, continuous filaments extruded from naturally flame-retardant basalt beads were examined as substitutes for asbestos fibers in almost all their applications. It is claimed that basalt fiber products offer similar properties to S-2 glass fibers at a price between glass S-2 and E glass and can offer manufacturers a cheaper alternative to carbon fiber products.

Basalt is an igneous volcanic rock. It is used as a raw material for the production of basalt fiber (for the production of heat and sound insulating materials, composite basalt reinforcement, for example). Mats of basalt fiber have an excellent thermal conductivity, hygroscopicity, and chemical resistance; in addition, it does not burn. Used in many industries, including mechanical engineering, as well as heat insulation material in the construction and other human activities (Kim and Lee, 2010; Asdrubali et al., 2014; Wand and Torng, 2001; Pompoli, 2004; Papadopoulos, 2005; Timoshenko et al., 1985). Materials reinforced with basalt fiber are highly resistant to weathering (including ultraviolet light), crashes (in crushed form, basalt fiber is also a part of mixture in concrete), corrosion with prolonged lifespan compared to steel, creating more durable structures with lower transportation costs due to lighter materials (lighter than reinforced concrete or metal poles) and easier handling which is suitable for mining industry, for example, for creating reinforcements for mining shafts (Lopresto et al., 2011). These features open up access to new technologies, results of scientific studies with these materials are applicable at world level.

The competitive advantages of materials reinforced with basalt fiber include:
- three times more durable than steel;
- no corrosion of the material;
- one-quarter of steel weigh;
- lower shipping costs;
- more economical to build high constructions;
- material lifespan is over 100 years;
- heat resistance 700 ° C and short-term, up to 1000 ° C (Buratti et al., 2013; Moretti et al., 2014; Buratti et al., 2014; Fabian et al., 2015; ASTM C518-10, 2003; EN ISO 12667, 2001; ISO 10534-2, 1998)

Areas of the usage of the basalt fiber are mainly the construction industry and especially mining. However, in the production of basalt fiber cloths, so-called non-fibrous inclusions are formed, which are bunches of molten original basalt filament. Their quantitative content depends on the perfection of the technological process of obtaining basalt fiber. In any case, these inclusions reduce the quality of the products and, due to their barbs, can

[1] *Anri Elbakian, Boris Sentyakov, Kirill Sentyakov*, Department of Mechatronic Systems, Faculty of Quality Management, Kalashnikov Izhevsk State Technical University, Studencheskaya street, 7, 426069, Izhevsk, Russia, henry25@mail.ru, sentyakov@inbox.ru, la1030@mail.ru

[2] *Pavol Božek,* Institute of Production Technologies, Faculty of Materials Science and Technology in Trnava, Slovak University of Technology in Bratislava, Jána Bottu street, 25, 917 24, Trnava, Slovak Republic, pavol.bozek@stuba.sk

[3] *Ivan Kuric,* Department of Automation and Production Systems, Faculty of Mechanical Engineering, University of Žilina, Univerzitná 8215/1, 010 26 Žilina, Slovak Republic, ivan.kuric@fstroj.utc.sk

lead to injuries, especially of the mucous membrane. It was found in research (Biderman, 1980) that affecting basalt fiber canvases by sound waves of the acoustic field, non-fibrous inclusions are falls from them. The task of modeling this phenomenon and process is worthwhile.

Figure 1 shows the scheme of basalt fiber in the form of an oscillatory system. The elementary fiber can be mistaken for an elastic beam located on adjacent curved fibers. Let us assume that on such fibers the non-fibrous excess inclusions having different geometric shapes and different masses are held by the forces of natural adhesion. Moreover, elementary fibers with non-fibrous inclusions attached to them are affected by the acoustic field. This research is done on the basis of the considered general theoretical principles of the investigation of the oscillatory system (Biderman, 1980; Bolotin, 1978; Makarov, 1982; Mensky, 1982; Uysal, 2013; Cavus, 2013).

Further below we will build a mathematical model of the process of sound impact on the considered system of interacting bodies connected by an elastic coupling (Figure 1).
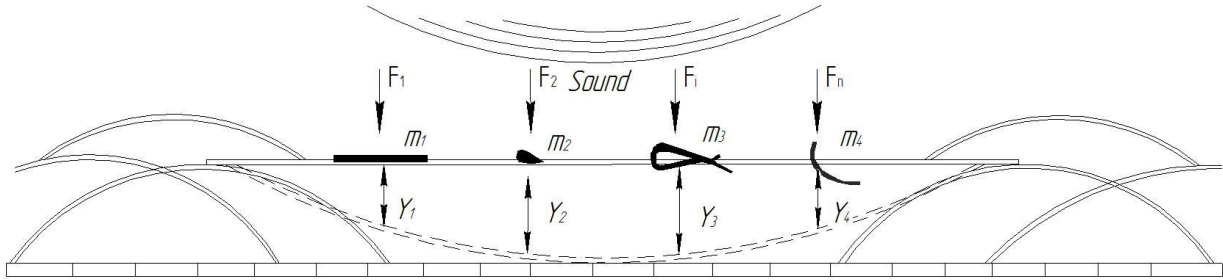
Fig. 1. The calculation scheme.

In Figure 1: m is the mass of non-fibrous inclusion, kg; c is the adhesion stiffness, N.m^{-1}; a is the damping coefficient (for energy losses due to viscous friction), kg. s^{-1}; y is the displacement of non-fibrous inclusions from the static equilibrium position, m; x is the displacement of the elastic base under the action of the driving force of the sound wave, m.

Consider the balance of power, acting on each of the four masses. We take Newton's second law as a basis. In this model, two forces are defined:

- the force of elastic resistance proportional to the movement,
- proportional to the speed of movement the force of elastic resistance.

According to the scheme for calculating the equilibrium equation of four forces (figure 1), we obtain a system of four differential equations in Eq. 1.

$$\begin{cases} m_1 y_1'' = c(x - y_1) + c(y_2 - y_1) + a(x' - y_1') + a(y_2' - y_1') \\ m_2 y_2'' = c(y_1 - y_2) + c(y_3 - y_2) + a(y_1' - y_2') + a(y_3' - y_2') \\ m_3 y_3'' = c(y_2 - y_3) + c(y_4 - y_3) + a(y_2' - y_3') + a(y_4' - y_3') \\ m_4 y_4'' = c(x - y_4) + c(y_3 - y_4) + a(x' - y_4') + a(y_3' - y_4') \end{cases} \tag{1}$$

The following second-order differential equations Eq. 2 can describe the free movement of each mass separately.

$$m_i y_i'' + a y_i' + c y_i = 0 \tag{2}$$

Or in the form of a typical oscillatory link (Makarov, 1982) of the dynamic system (Eq. 3).

$$T_i^2 y_i'' + 2T_i \xi_i y_i' + y_i = 0 \tag{3}$$

Where T_i is the period of free oscillations (or time constant), s;
   ξ_i - the damping coefficient ($0 < \xi_i < 1$).

These parameters in the joint consideration of Eq. 2 and Eq. 3 are the following (Eq. 4, Eq. 5):

$$T_i = \sqrt{\frac{m_i}{c}} \tag{4}$$

$$a = 2T_i \xi_i c \tag{5}$$

Then the fundamental frequency of each of the four elements is determined from the known formula (Makarov, 1982):

$$\omega_i = \frac{\sqrt{1-\xi_i^2}}{T_i} = \frac{\sqrt{4m_ic-a^2}}{2m_i} \tag{6}$$

Using an analytical method for solving the system of Eq. 1, we get one linear differential equation. It has constant coefficients of the eighth order. The further task causes certain difficulties, since it involves the consideration of various solutions for real and complex roots, finding the roots of the characteristic equation of the eighth degree.

It is necessary to investigate the object in the frequency domain, as well as to consider alternative ways to solve the system (Eq. 1). It is proposed to use the methods of Makarov (Makarov, 1982) Automatic Control Theory (TAU). Applying the Laplace transforms, and going over to the images (Eq. 7), the system (Eq. 1) can be represented in the form (Eq. 8):

$$\begin{cases} y_i'' \to p^2 Y_i \\ y_i' \to p Y_i \end{cases} \tag{7}$$

$$\begin{cases} m_1 p^2 Y_1 + 2apY_1 + 2cY_1 = (c+ap)(X+Y_2) \\ m_2 p^2 Y_2 + 2apY_2 + 2cY_2 = (c+ap)(Y_1+Y_3) \\ m_3 p^2 Y_3 + 2apY_3 + 2cY_3 = (c+ap)(Y_2+Y_4) \\ m_4 p^2 Y_4 + 2apY_4 + 2cY_4 = (c+ap)(Y_3+X) \end{cases} \tag{8}$$

Or as a system of operator equations with transfer functions (Eq. 9):

$$\begin{cases} Y_1 = W_1(X+Y_2) \\ Y_2 = W_2(Y_1+Y_3) \\ Y_3 = W_3(Y_2+Y_4) \\ Y_4 = W_4(Y_3+X) \end{cases} \tag{9}$$

The following equation (Eq. 10) expresses a mathematical model of the structural elements of a dynamic system by defining the transfer function of the operator.

$$\begin{cases} W_1 = \frac{c+ap}{m_1 p^2 + 2ap + 2c} \\ W_2 = \frac{c+ap}{m_2 p^2 + 2ap + 2c} \\ W_3 = \frac{c+ap}{m_3 p^2 + 2ap + 2c} \\ W_4 = \frac{c+ap}{m_4 p^2 + 2ap + 2c} \end{cases} \tag{10}$$

Then, solving the system (Eq. 9) about Y_i for a given X, we obtain a system solution (Eq. 1) for all masses in the following operator form (Eq. 11).

$$Y_i = W_{pi}(p)X \tag{11}$$

We can obtain an analytical solution to the problem through the inverse Laplace transform.

Applying a complex transfer function (Eq. 12), according to the known formulas (Makarov, 1982; Sentyakov, 2004; Timofeev, 2004; Jasenek et al., 2012) we have the amplitude-frequency $A(\omega)$ and the phase-frequency $\varphi(\omega)$ characteristics (Eq. 12):

$$\begin{cases} W_P(\omega i) = Re(\omega) + Im(\omega) \cdot i \\ A(\omega) = |W_P(\omega i)| = \sqrt{Re(\omega)^2 + Im(\omega)^2} \\ \varphi(\omega) = arg\,(W_P(\omega i)) = arctg(Im(\omega)/Re(\omega)) \end{cases} \tag{12}$$

As the square roots of the eigenvalues of the matrix (Eq. 13) coefficients of the original (Eq. 1) undamped ($\xi_i = 0$, $a_i = 0$) differential equations system, the critical frequencies can be calculated without amplitude response.

$$\begin{bmatrix} \dfrac{-2c}{m_1} & \dfrac{c}{m_1} & 0 & 0 \\[2mm] \dfrac{c}{m_2} & -\dfrac{2c}{m_2} & \dfrac{c}{m_2} & 0 \\[2mm] 0 & \dfrac{c}{m_3} & -\dfrac{2c}{m_3} & \dfrac{c}{m_3} \\[2mm] 0 & 0 & \dfrac{c}{m_4} & \dfrac{-2c}{m_4} \end{bmatrix} \tag{13}$$

Material and Methods

Calculate the eigenvalues of the matrix of the fourth order. This will again require the solution of high order algebraic equations. We will use one of the many application software solutions for such tasks (Shaiks, 2018; Haque, 2018; Kuzmin et al., 2015).

The dynamic characteristic of the system is obtained in accordance with the proposed model. The following physical quantities are used:

- elementary fiber diameter $d = 0.003$ mm;
- elementary fiber length $L = 35$ mm;
- size (the ball diameter) of inclusions $v_1 = 0.3$, $v_2 = 0.1$, $v_3 = 0.5$, $v_4 = 0.2$ mm;
- Basalt density $p = 2300$ kg . m^{-3} = 2.3 mg . mm^{-3};
- Basalt elasticity modulus $E = 100$ GPa.

Then the fiber rigidity coefficient is the following (Eq. 14):

$$c = E \cdot \frac{S}{L} = 20.20 \frac{\text{H}}{\text{м}} = 2020 \; mg \, . \, mm^{-1} \tag{14}$$

Where S - the elementary fiber cross-sectional area for the known d.

The inclusion masses for known v and par respectively equal to $m_1 = 0.01035$, $m_2 = 0.00038$, $m_3 = 0.04792$, $m_4 = 0.00307$ mg.

The damping coefficient affects the amplitude of the mass oscillation and is assumed to be a = 1 mg . s^{-1}. It does not affect the critical frequency.

The following critical frequencies of the system have been obtained with respect to the matrix (13) were thus $\omega K_1 = 517$, $\omega K_2 = 86$, $\omega K_3 = 29$, $\omega K_4 = 183$ Hz.

The natural frequencies of the individual masses according to the formula (6) are respectively equal to $\omega_1 = 70$, $\omega_2 = 301$, $\omega_3 = 33$, $\omega_4 = 127$ Hz.

Figure 2 shows the system solution (Eq. 1) with frequency impact at the lower critical frequency $x = \sin(29t)$.
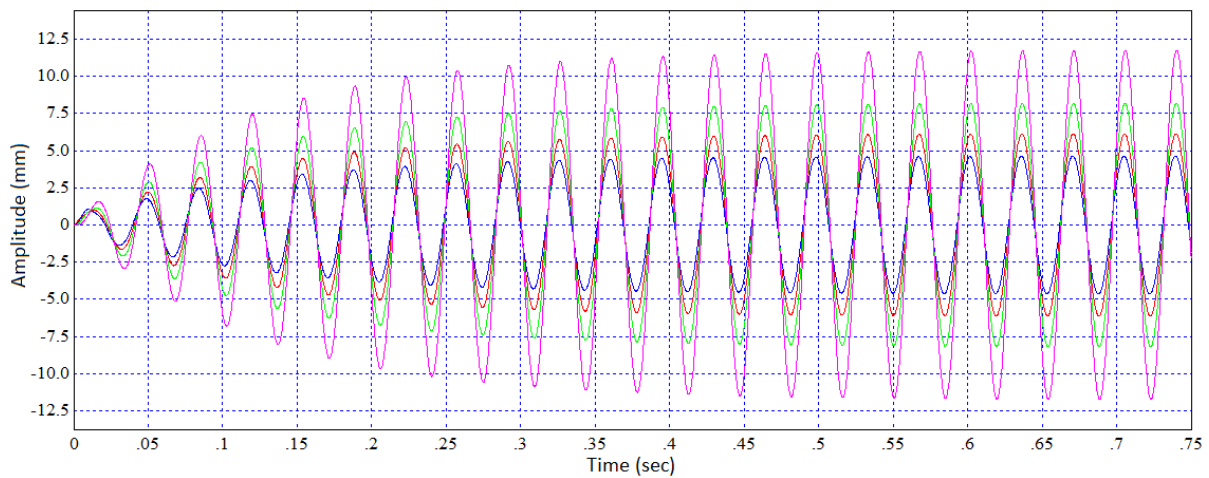
Fig. 2. Amplitude mode for x = sin(29t).

Figure 3 shows the system solution (Eq. 1) with frequency impact at the second critical frequency $x = \sin(86t)$.
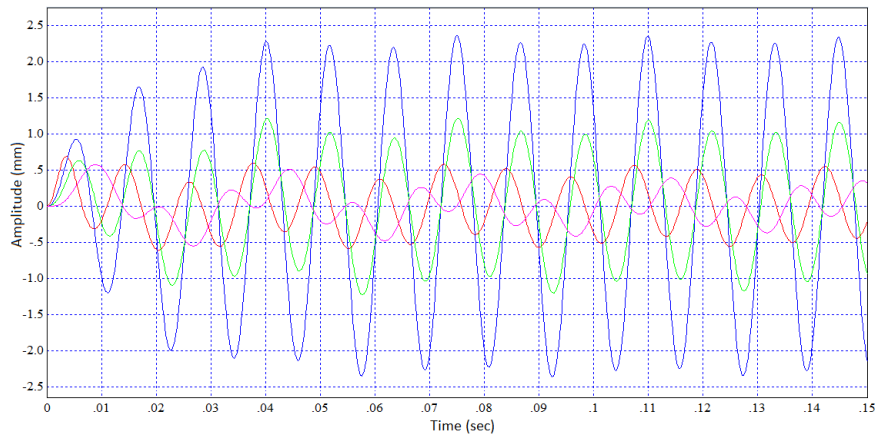
Fig. 3. Amplitude mode for x = sin (86t).

Figure 4 shows the system solution (Eq. 1) with frequency impact at the next critical frequency $x = \sin (183t)$.
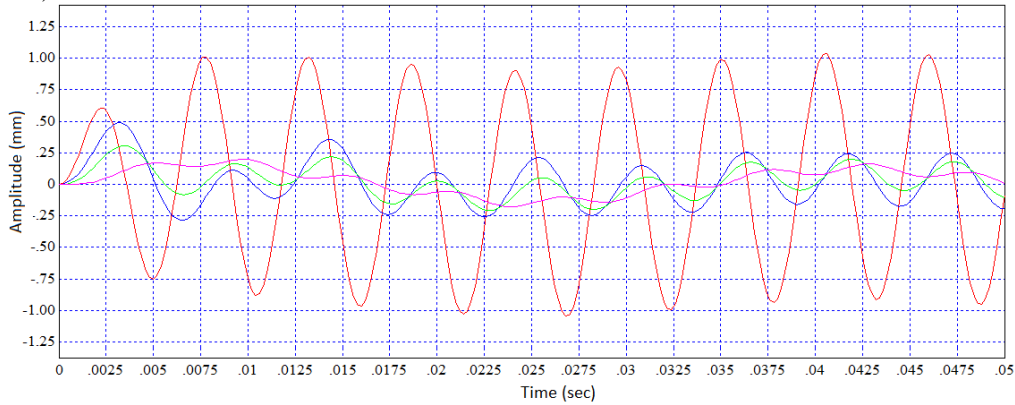
Fig. 4. Amplitude mode x = sin(183t).

The amplitude-frequency characteristics for all masses, calculated from formulas (Eq. 12) is shown in Figure 5.
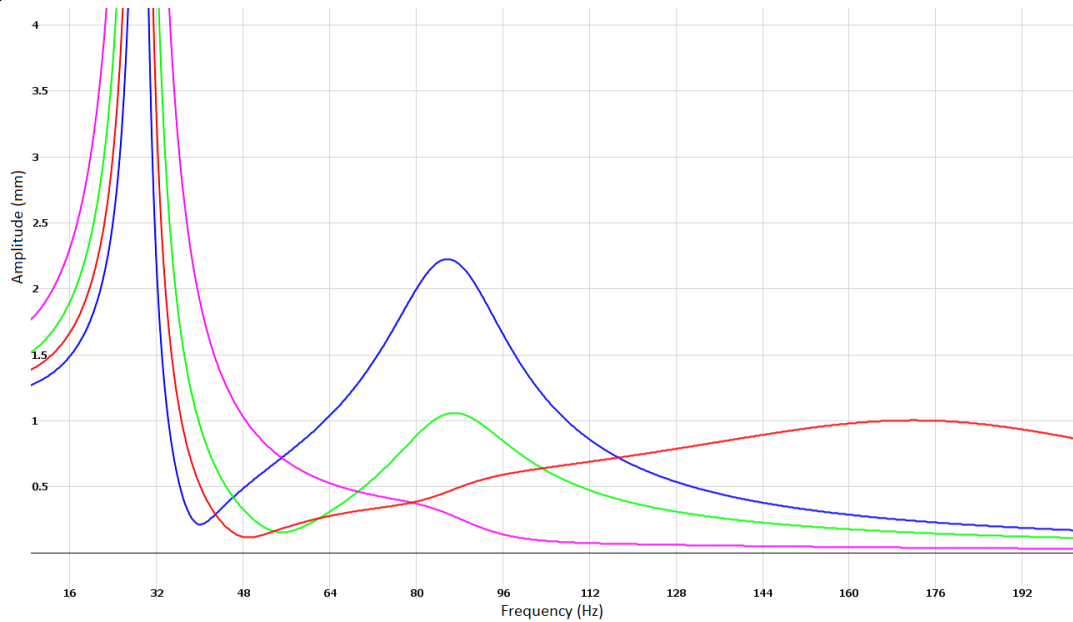
Fig. 5. Frequency dependence of the amplitude.

The largest resonance amplitude is observed at the very first (lowest) critical frequency of the system as shown in Figures 2 and 5.

The inertia force that detaches the inclusion from the fiber depends not only on the amplitude but also on the oscillation frequency (Bury et al., 2017; Akhmatova, 1980):

$$F_i = m_i A_i \omega^2 \tag{15}$$

The dependence of the detachment force of all masses on the frequency, calculated by the formula (Eq. 15) is shown in Figure 6.
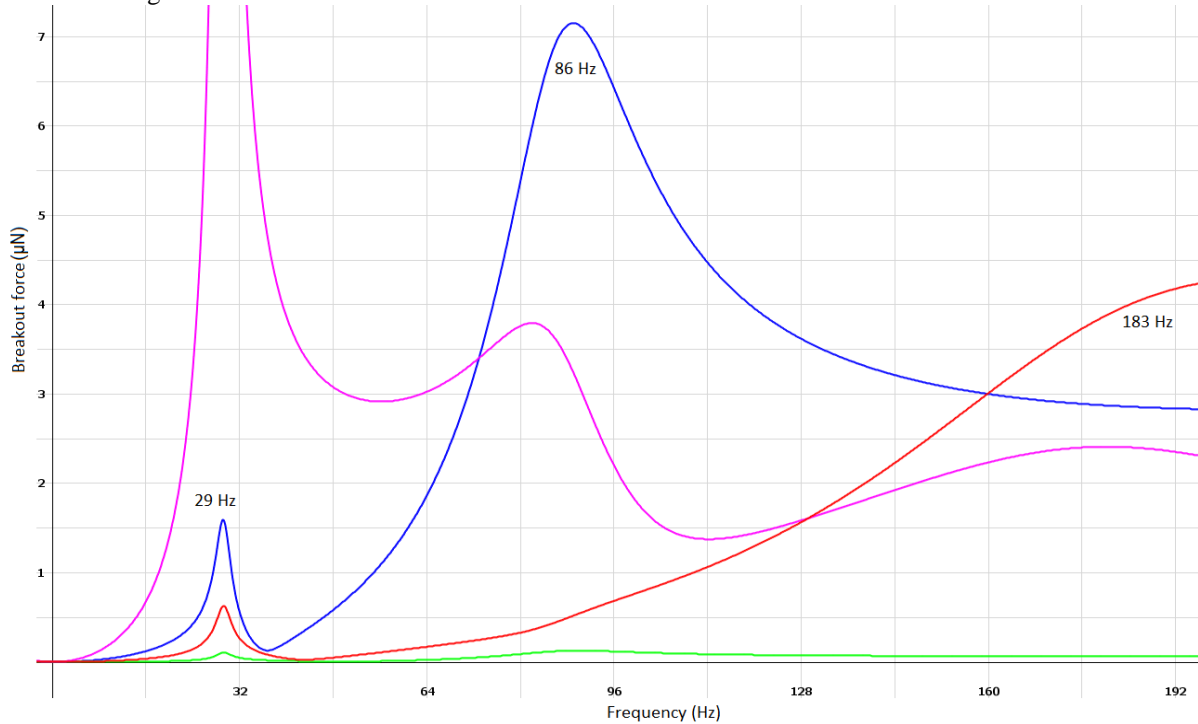
Fig. 6. Dependence of separation force on the frequency.

So, for example, for the first mass (the blue line in the graphs), the amplitudes at first (ascending) three critical frequencies will be 5, 2.3 and 0.2 mm (Fig. 2, 3, 4 and 5). The corresponding detachment forces (Fig. 6) will be 2.5, 7 and 3 μN. The greatest detachment force corresponds to the highest value of the product of mass, amplitude, and the square of cyclic frequency (Eq. 15). Therefore, it appears not at the largest amplitude and not the highest frequency.

Experimental study for the acoustical treatment process of the superthin basalt fiber canvas (Boczar, 2003; Ribero, 2003; Kriven, 2016).This research aims to confirm the benefits and find rational parameters of the acoustical treatment process of the formed primary canvases. The reasons for the formation of non-fibrous inclusions in canvases made from superthin basalt fiber obtained by duplex technology are known from (Jasenek et al. 2012). Below in Figure 7 is the experimental installation scheme for studying the acoustic field effect on superthin basalt fiber samples. The sound source is a loudspeaker 1 type BD 93, with a diffuser 120 mm in diameter, power 40 W and a working frequency range of generated sound vibrations from 38 to 18000 Hz. The loudspeaker is connected to a sound generator of type G3-33, providing a frequency change in the audio range from 20 to 20,000 Hz with an output voltage of up to 14 V.
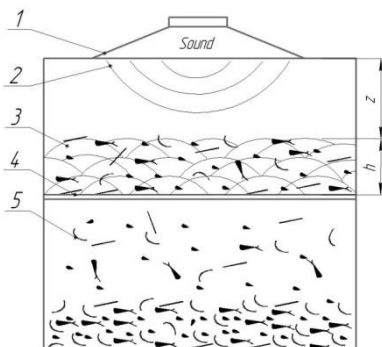
Fig. 7. Installation for acoustic treatment of basalt fiber canvas samples:
1 - sound source, 2 - sound wave, 3 - basalt canvas, 4 - grid, 5 - non-fibrous inclusions,
h - the thickness of canvas, z-distance from the sound source.

To measure the weight of samples of superthin basalt fiber canvases and the mass of non-fibrous inclusions falling out of them under the sound influence, electronic laboratory scales GH-252 with a division value of 0.1 mg were used. The test samples had the same thickness h and were located at a distance z from the loudspeaker on a wire grid with a diameter of 2 mm in increments of 20 mm in one direction and 40 mm in the other 4 (Fiore et al., 2015).

In Figure 7, the tests were carried out as follows. Under the influence of sound vibrations 2 from the lower surface of the basalt fiber canvas sample 3, non-fibrous inclusions 5 did actually begin to separate.

The first preliminary experiments showed that non-fibrous inclusions do not fall out of the canvas under the sound influence in the frequency range from 260 Hz to 20 kHz, and an essential reaction is observed only in the sound frequency range from 40 to 160 Hz. The sound level was 118 ± 2 dB.

Sixty-five samples of superthin basalt fiber canvases with sizes 150 x 150 x 8 to 10 mm and density 13.2 to 15.1 kg.m^{-3} were prepared for further experiments. All experiments were carried out in five series - when every five samples were exposed to sound of different frequencies - from 40 Hz every 10 Hz to 160 Hz. The sound level was 118 ± 2 dB. In these experiments, the total mass of all non-fibrous inclusions fallen out under the influence of sound from each sample was measured without differentiating them by mass and shape (Fig. 8).
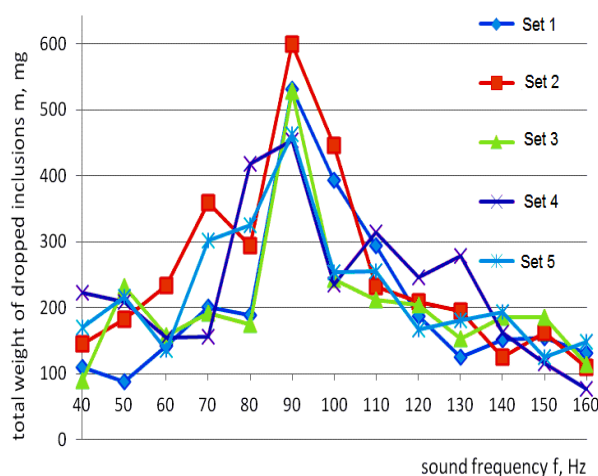
Fig. 8. The total mass dependence of all non-fibrous inclusions, fallen out under the sound field influence, on the sound frequency.

Results and Discussion

The results of the experiments are shown in Figure 8, from which it follows that the largest number of non-fibrous inclusions, according to their total mass, are separated from the canvas samples under the sound influence at a frequency of 90 Hz.

It should be noted that the total mass of the fallen non-fibrous inclusions determined in these experiments does not allow us to judge with confidence the optimal parameters of acoustic processing-the frequency and the sound level at which the greatest number of inclusions from the canvas falls out since the inclusions proportion in different samples vary. It was not possible to prepare canvas samples with the same number of non-fibrous inclusions contained in them due to the fact that the processes of inclusions formation have a random character.

Strictly speaking, the acoustic treatment efficiency of the considered articles can be judged if the mass fractions of the non-fibrous inclusions contained in the samples before and after the acoustic treatment are determined (Timoshenko et al., 1985). For this purpose, the efficiency index of the basalt fiber canvases acoustic treatment is introduced - the reduction coefficient of the non-fibrous inclusions content in the canvas sample KNI determined by the ratio:

$$K_{NI} = \frac{\omega_0}{\omega_1},$$

(16)

Tab. 1. Mass fraction of non-fibrous inclusions (NI) in superthin basalt fiber canvases before and after acoustic treatment.

No. Experiment	The canvas mass before treatment M_0, (mg)	The fallen outNI mass m_2(mg)	The canvas mass after treatment M_1, (mg)	The remaining NI mass m1, (mg)	Mass fraction of NI in the canvas before treatment ω_0, %	Mass fraction of NI in the canvas after treatmentω, %	The reduction coefficient of NI mass fraction KNI	The average value <KNI>
Sound frequency 70 Hz level 100 dB, generator voltage U = 12 V, exposure time t = 40 s								
1	998.7	5.8	992.9	76.3	8.22	7.68	1 070	
2	897.9	4.5	893.4	64.3	7.66	7.20	1 064	1 087
3	639.5	8.0	631.5	64.6	11.35	10.23	1 109	
4	1501.6	22.9	1478.7	187.1	14.02	12.69	1 105	
Sound frequency 90 Hz level 100 dB, generator voltage U = 12 V, exposure time t = 40 s								
5	1126.2	14.6	1111.6	88.8	9.18	7.99	1 149	
6	773.3	7.1	766.2	40.8	6.19	5.32	1 164	1 145
7	771.2	3.7	767.5	29.5	4.30	3.84	1 120	
8	682.0	13.1	668.7	78.18	13.41	11.69	1 147	
Sound frequency 110 Hz, level 100 dB, generator voltage U = 12 V, exposure time t = 40 s								
9	425.1	4.0	421.1	39.7	10.28	9.43	1 090	
10	960.6	4.1	956.5	70.2	7.73	7.34	1 053	1 070
11	825.2	4.5	820.7	54.3	7.13	6.62	1 077	
12	1037.2	4.3	1032.9	84.2	8.63	8.15	1 059	
Sound frequency 70 Hz, level 118 dB, generator voltage U = 12 V, exposure time t = 40 s								
13	606.0	41.7	564.3	42.7	13.93	7.57	1 840	
14	1045.8	73.4	972.4	86.4	15.28	8.89	1 719	1 723
15	434.7	24.3	410.4	37.8	14.29	9.21	1 552	
16	448.5	34.6	413.9	37.2	16.00	8.99	1 780	
Sound frequency 90 Hz level 118 dB, generator voltage U = 12 V, exposure time t = 40 s								
17	582.9	42.4	540.5	29.8	12.39	5.5	2 253	
18	996.9	44.3	952.3	53.6	9.82	5.63	1 744	2 368
19	704.9	37.7	667.2	32.2	9.92	4.83	2 054	
20	482.7	85.1	397.6	27.0	23.22	6.79	3.42	
Sound frequency 110 Hz, level 118 dB, generator voltage U = 12 V, exposure time t = 40 s								
21	805.1	40.3	764.8	29.8	8.71	3.90	2.233	
22	545.2	16.4	528.8	22.3	7.10	4.22	1 682	1 850
23	648.3	26.8	621.5	33.3	9.27	5.36	1 729	
24	697.1	40.6	656.5	47.0	12.57	7.16	1 756	

where ω_0 and ω_1- the mass fraction of non-fibrous inclusions in the sample before and after treatment (%), respectively, which are in turn determined by the expressions:

$$\omega_0 = 100 * \frac{m_0}{M_0}, \qquad\qquad \omega_1 = 100 * \frac{m_1}{M_1}, \qquad\qquad (17)$$

Where m_0 and m_1 are respectively the mass of non-fibrous inclusions in the sample before and after treatment, M_0 and M_1 are, respectively, the mass of the sample before and after treatment. The values of m_0, m_1, M_0, M_1 were obtained using the electronic laboratory scale GH-252 with a division value of 0.1 mg.

For the next series of experiments twenty-four samples with dimensions of 150x150x8 to 10 mm and a density of 13.2 ... 15.1 kg / m^3 were prepared in order to determine the reduction coefficient of the non-fibrous inclusion content in the canvas sample *KNI* (Eq. 16, Eq. 17) at the frequencies of the applied sound field f = 70 Hz, f = 90 Hz and f = 100 Hz and the sound level is L = 100 dB and L = 118 dB, respectively. The measurements results of m_0, m_1, M_0, M_1, and calculations of ω_0, ω_1, and m_2 (the mass of non-fibrous inclusions fallen out from the superthin basalt fiber canvas in the process of acoustic treatment) are presented in Table 1.

As can be seen from the Table 1, the mass of non-fibrous inclusions fallen out of the samples under the sound influence is proportional to the sound level L, since the *KNI* index at a sound level of L = 118 dB is much higher in comparison with the analogous index at a sound level of L = 110 dB. Just as in the previous experiments, the maximum decrease in the non-fibrous inclusions content in the samples after acoustic treatment with a frequency of 90 Hz is observed, while the mass fraction of non-fibrous inclusions in basaltic fiber canvases at an L = 118 dB sound level decreases by an average of 2.4 times.

For a better understanding of the acoustic treatment practical benefits, we introduce one more efficiency indicator - the mass fraction percentage of non-fibrous inclusions fallen out during processing, from the mass of all inclusions in the sample before treatment with NI$_\%$:

$$NI_\% = 100 * \frac{m_2}{m_1+m_2}, \qquad\qquad (18)$$

where m_1 is the mass of non-fibrous inclusions in the sample remaining after processing, m_2 is the mass of non-fibrous inclusions fallen out during processing.

Using the known formulas (Eq. 19, Eq. 20, Eq. 21, Eq. 22, Eq. 23) for processing the results and determining the error (Sentyakov, 2004; Timofeev, 2004) and formula 3, we can calculate the limits of the $NI_\%$ value for each of the six combinations (f = 70 Hz and L = 110 dB , f = 79 Hz and L = 110 dB, f = 110 Hz and L = 110 dB, f = 70 Hz and L = 118 dB, f = 90 Hz and L = 118 dB, f = 110 Hz and L = 118 dB) of the sound field output parameters, presented in Table 1.

$$< NI_\% > = \frac{\Sigma NI_{\%i}}{n}, \qquad\qquad (19)$$

where $<NI_\%>$ is the arithmetic average of the mass fraction percentage of non-fibrous inclusions fallen out during processing, on the mass of all inclusions in the sample before processing, $\Sigma NI_{\%i}$ is the sum of the values of all the experiments, n is the number of experiments,

$$\Delta NI_{\%i} = < NI_\% > - NI_{\%i}, \qquad\qquad (20)$$

where $\Delta NI_{\%i}$ – the deviation of each experiment value from the average,

$$S_{<NI_\%>} = \sqrt{\frac{\Sigma(\Delta NI_{\%i})^2}{n(n-1)}}, \qquad\qquad (21)$$

where $S_{<NI_\%>}$ – confidence interval,

$$\Delta NI_\% = S_{<NI_\%>} \times t, \qquad\qquad (22)$$

where $\Delta NI_\%$ is the deviation, t is the coefficient of the student (3.2 for reliability p = 0.95), that is, how many times it is necessary to increase the standard confidence interval, so that for a certain number of tests n get the reliability of p,

$$NI_\% = < NI_\% > \pm \Delta NI_\%, \qquad\qquad (23)$$

The results of the calculations are listed in Table 2.

Tab. 2. The mass fraction percentage of non-fibrous inclusions NI$_\%$ fallen out during acoustic processing of basalt fiber canvases.

No. of experiments	Sound level L, dB	Soundwave frequency f, Hz	NI$_\%$, %
1, 2, 3, 4	100	70	5-12
5, 6, 7, 8	100	90	11-16
9, 10, 11, 12,	110	110	3,5-10
13,14,15,16	118	70	38-53
17,18,19,20	118	90	38-79
21,22,23,24	118	110	37-58

Conclusions

The widespread of the $NI_\%$ is explained by the different samples heterogeneity; it is impossible to select two samples even with an approximate identical content of the amount or mass fraction of non-fibrous inclusions. However, a certain regularity is observed (Biderman, 1980). As can be seen from Table 2, the mass fraction of the fallen non-fibrous inclusions $NI_\%$ in the acoustic treatment process from the total mass of non-fibrous inclusions, that were contained in the sample before processing, is proportional to the sound level L. In the concluded experiments, the maximum number of $NI_\%$ heavily depended on the exposed sound frequency, at f = 90 Hz which was achieved at a sound level of L = 118 dB the fraction of inclusions can reach up to 80 %.

Thus, as a result of an experimental study of the acoustic treatment process, the application of this treatment process for reduction of the non-fibrous inclusions content in primary superthin basalt fiber canvases has been confirmed, which also improves the working conditions for people working with basalt fiber canvases. Following recommendations for further study of non-fibrous inclusions separation by means of acoustic vibrations and determination of rational parameters for the application of the acoustic treatment process into the mining industry are suggested:

- investigation of the sound field distribution based on its distance from the acoustic vibrations source;
- investigation of the necessary processing time depending on the created sound level at the interaction point of the sound field with the primary canvas;
- further study of the vibrational properties of individual particles in non-fibrous inclusion separation from the basalt fiber canvas using acoustic vibrations, in order to accurately estimate the reason for the mass of the individual inclusions to differ greatly among themselves at a certain frequency level, even though the sound effect frequency coincides with the natural frequency of oscillation of non-fibrous inclusions by the appearance of a physical resonance;
- the most effective acoustic processing in this study has been found to be at a frequency of 90 Hz;
- the design of acoustic processing equipment has to provide the possibility to adjust the distance from the sound source to the sample surface within a distance that will provide a sound level at the interaction point at a level not lower than 118 dB;
- the conveyor speed and the number of loudspeakers must allow for the sample surface to be exposed to the sound for 20 to 40s.

References

Akhmatova, A. S. (1980). Laboratorniy practicum pofizike (Laboratory practical work on physics). *Moscow: Vishayashkolaizdt.*

Asdrubali, F., D'Alessandro, F., Mencarelli and Horoshenkov, K. V. (2014). Sound absorption properties of tropical plants for indoor applications. The 21st International Congress on Sound and Vibration, 13-17 July 2014, Beijing, *China.*

ASTM C518-10. (2003). Standard Test Method for Steady-State Thermal Transmission Properties by Means of the Heat Flow Meter Apparatus; ASTM: USA: West Conshohocken, PA.

Biderman V.L. (1980) Theory of Mechanical Oscillations: A Textbook for High Schools. *M: High School, 408 p., Ill.*

Biderman, V. L. (1980). Theory of Mechanical Oscillations: *A Textbook for High Schools*.

Boczar, T. (2003) Time-Frequency Analysis of Acoustic Emission Pulses Generated by Partial Discharges, *Journal of Electrical Engineering, (54) 63-68.*

Bolotin, V. V. (1987). Vibrations in technology: Handbook. In six Volumes. *Moscow: Mashinostroenie*.

Buratti, C., Moretti, E., Belloni, E. and Agosti, F. (2014). Development of Innovative Aerogel Based Plasters: Preliminary Thermal and Acoustic Performance Evaluation. Sustainability 2014(6) 5839-5852. [online]. [2015-02-03]. Available at : http://www.enea.it/it/produzione-scientifica/EAI/anno-2011/indice-world-view-3-2011/basalt-fiber-from-earth-an-ancient- material-for innovative-and-modern-application//

Buratti, C., Moretti, E., Belloni, E. and Cotana, F. (2013). Unsteady simulation of energy performance and thermal comfort in non-residential buildings. *Building and Environment 2013(59) 482-491*.

Bury, P., Hardoň, Š., Kobayashi, H. and Imamura K. (2017). Investigation of deep defects in nanocrystalline-Si/Si interfaces using acoustic spectroscopy. *Journal of Electrical Engineering 2017(68) 1335 – 3632*.

E N ISO 12667. (2001). Thermal Performance of Building Materials and Products-Determination of Thermal Resistance by Means of Guarded Hot Plate and Heat Flow Meter Methods-Products of High and Medium Thermal Resistance; *ISO: Geneva, Switzerland*.

Fabian, M., Boslai, R., Ižol, P., Janeková, J., Fabianová, J., Fedorko, G., and Božek, P. (2015). Use of parametric 3D modelling - tying parameter values to spreadsheets at designing molds for plastic injection. *Manufacturing Technology 2015 (15) 24-31*

Fiore, V., Scalici, T., Di Bella, G., Valenza, A. (2015). A review on basalt fibre and its composites. Composites Part B*: Engineering Volume 74, 1 June 2015, Pages 74-94*.

Huang, S. Z. C and Pan, Y-Ch. (2015). Automated visual inspection in the semiconductor industry: A survey. *Computers in Industry, 2015 (66) 1-10*.

ISO 10534-2. (1998). Acoustics-Determination of Sound Absorption Coefficient and Impedance in Impedance Tubes-Part 2: Transfer-Function Method*; ISO: Geneva, Switzerland*.

Jasenek, J., Korenko, B. and Červeňová, J. (2012). Fiber optic sensor for the space distribution measurement of magnetic field. *Journal of Electrical Engineering 2012 (63) 23-26*.

Kemal Ozfirat, M. (2015). Selection of tunneling machines in soft ground by fuzzy analytic hierarchy process. *Acta Montanistica Slovaca 2015(20) 98-109*.

Kim, H. K. and Lee, H. K. (2010). Influence of cement flow and aggregate type on the mechanical and acoustic characteristics of porous concrete. *Applied Acoustics 2010(71) 607-615*.

Kuzmin, K. L., Gutnikov, S. I., Zhukovskaya, E. S. and Lazoryak, B. I. (2017). Basaltic glass fibers with advanced mechanical properties. *Journal of Non-Crystalline Solids 2017(476) 144-150*.

Lopresto, V., Leone, C. and De Iorio, I. (2011). Mechanical characterisation of basalt fibre reinforced plastic. *Composites Part B: Engineering 2011(42) 717-723*.

Makarov, I. M. and Mensky, B. M. (1981). Linear automatic systems. *Mechanical Engineering 1981(23) 221-232*.

Moretti, E., Zinzi, M. and Belloni, E. (2014). Polycarbonate panels for buildings: Experimental investigation of thermal and optical performance. *Energy and Building 2014(70) 23-35*.

Papadopoulos, A. M. (2005). State of the art in thermal insulation materials and aims for future developments. *Energy Build. 2005(37) 77-86*.

Pompoli, F. (2004). Studio di modelli di previsione delle proprietà fisico-acustiche, di materiali in lana di roccia Rockwool, *Relazione Tecnica*.

Ribero, D., Kriven, W.M. (2016) Properties of Geopolymer Composites Reinforced with Basalt Chopped Strand Mat or Woven Fabric. *Journal of the American Ceramic Society Volume 99, Issue 4, 1 April 2016, Pages 1192-1199.*

Sentyakov, B. A. and Timofeev, L. V. (2004). Tehnologia proizvodstva teploizolyacionnih materialov na osnove basaltovogo volokna (Technology of production of thermal insulation materials based on basalt fiber). *Izhevsk: ISTU* .

Shaikh, F. and Haque, S. (2018). Behaviour of Carbon and Basalt Fibres Reinforced Fly Ash Geopolymer at Elevated Temperatures. *International Journal of Concrete Structures and Materials. 2018 (12) 35*.

Timoshenko S.P, Young D.H. and Weaver, U. (1985). Oscillations in engineering. / Transl. from English. Korneyuchuk, L. G., Ed. Grigoluk, E. I. - M. (1985). *Mechanical Engineering 1985(27) 243-254*.

Uysal, O., Cavus, M.: Effect of a pre-split plane on the frequencies of blast induced ground vibrations. *Acta Montanistica Slovaca 2013(18) 101-109*.

Wang, C. N. and Torng, J. H. (2001). Experimental study of the absorption characteristics of some porous fibrous materials. *Applied Acoustics 2001 (62) 447- 459*.